

A new spatially scanning 2.7 μm laser hygrometer and new small-scale wind tunnel for direct analysis of the H_2O boundary layer structure at single plant leaves

K. Wunderle · U. Rascher · R. Pieruschka ·
U. Schurr · V. Ebert

Received: 20 April 2014 / Accepted: 15 October 2014 / Published online: 7 November 2014
© Springer-Verlag Berlin Heidelberg 2014

Abstract A new spatially scanning TDLAS in situ hygrometer based on a 2.7- μm DFB diode laser was constructed and used to analyse the water vapour concentration boundary layer structure at the surface of a single plant leaf. Using an absorption length of only 5.4 cm, the TDLAS hygrometer permits a H_2O vapour concentration resolution of 31 ppmv. This corresponds to a normalized precision of 1.7 ppm m. In order to preserve and control the H_2O boundary layer on an individual leaf and to study the boundary layer dependence on the wind speed to which the leaf might be exposed in nature, we also constructed a new, application specific, small-scale, wind tunnel for individual plant leaves. The rectangular, closed-loop tunnel has overall dimensions of 1.2×0.6 m and a measurement chamber dimension of 40×54 mm (H \times W). It allows to generate a laminar flow with a precisely controlled wind speed at the plant leaf surface. Combining honeycombs and a miniaturized compression orifice, we could generate and control stable wind speeds from 0.1 to 0.9 m/s, and a highly laminar and homogeneous flow with an excellent

relative spatial homogeneity of 0.969 ± 0.03 . Combining the spectrometer and the wind tunnel, we analysed (for the first time) non-invasively the wind speed-dependent vertical structure of the H_2O vapour distribution within the boundary layer of a single plant leaf. Using our time-lag-free data acquisition procedure for phase locked signal averaging, we achieved a temporal resolution of 0.2 s for an individual spatial point, while a complete vertical spatial scan at a spatial resolution of 0.18 mm took 77 s. The boundary layer thickness was found to decrease from 6.7 to 3.6 mm at increasing wind speeds of 0.1–0.9 m/s. According to our knowledge, this is the first experimental quantification of wind speed-dependent H_2O vapour boundary layer concentration profiles of single plant leaves.

1 Introduction

The earth's vegetation constitutes the functional interface between the atmosphere and the earth surface and greatly determines land–atmosphere gas exchange processes. Atmospheric water vapour emissions from plants are large and greatly dependent on the functional status of the vegetation. In the global water cycle, plant transpiration accounts for 64 % of the global precipitation recycling back to the atmosphere [1]. As water vapour is one of the most prominent greenhouse gases, it is important to understand the vapour fluxes from plants on different scales, from the single leaf to the global vegetation. In particular, the spatio-temporal variability of the water vapour exchange rates and the corresponding fluxes between phytosphere and atmosphere represent key elements for a reliable modelling of the weather and climate processes [2, 3]. Despite their high importance, transport

K. Wunderle (✉) · V. Ebert
Physical-Chemistry Institute (PCI), Ruprecht-Karls Universität
Heidelberg, Heidelberg, Germany
e-mail: karl.wunderle@alumni.uni-heidelberg.de

U. Rascher · R. Pieruschka · U. Schurr
Institute of Bio- and Geosciences (IBG), IBG-2 Plant Sciences,
Forschungszentrum Jülich, Germany

V. Ebert
Center of Smart Interfaces (CSI), Technische Universität
Darmstadt, Darmstadt, Germany

V. Ebert
Physikalisch-Technische Bundesanstalt (PTB), Braunschweig,
Germany

processes from a leaf through the boundary layer to the atmosphere are far from being completely understood on the various spatial scales and often have to rely on theoretical relations, which could not be verified so far. On the surface of plant leaves, the so-called stomata represent the microscopic pores with a size ranging between 10 and 30 μm [4]. The stomata can be considered as “gates” between the atmosphere and the leaf’s interior. Ultimately, stomata regulate the gas fluxes of CO_2 into and H_2O out of the leaf. Gas fluxes are measured with various measurement techniques across the various spatial scales. Gas exchange measurements on the ecosystem level can be performed with eddy covariance approaches [5] which provide bulk gas exchange fluxes but do not allow mechanistic studies of the governing processes. Chlorophyll fluorescence measurements, providing quantification of photosynthetic efficiency and an indirect indicator of gas fluxes, can be performed on different scales from leaf [6] to canopy [7, 8] and ecosystem scale [9]. Direct analysis of gas exchange can be performed with dedicated techniques on plants and leaves [10] or even at the level of single stomata [11]; however, these measurements can often only be performed under very artificial conditions. A better knowledge about stomatal control mechanisms is the key to model water vapour and CO_2 fluxes [12]. Validation experiments which mimic environmental conditions as closely as possible are therefore urgently needed to enhance the understanding of plant environment interaction.

A more detailed look on the transpiration of single plant leaves reveals that the gas exchange processes on the leaf surface are often spatially heterogeneous and highly dynamic [13] even under spatially homogeneous experimental conditions. In addition to the lateral heterogeneities of the gas exchange along the leaf surface, water vapour emission by the leaf also causes the formation of a vertical H_2O vapour concentration gradient perpendicular to the leaf surface, i.e. a boundary layer structure enriched with water vapour. This concentration boundary layer (CBL) determines the physical properties of the interface between the external free gas space and the air-filled intercellular spaces inside the leaf. According to Fick’s law, the CBL actuates the diffusional transport resistance and thus limits the flux of gaseous compounds into the atmosphere. While experimental data on the wind speed within the boundary layer are available [14], there is no direct measurement of the water vapour concentration profile within the boundary layer of a single leaf. Thus, the understanding of the boundary layer gas exchange processes is only based on theoretical descriptions of the H_2O vapour boundary layer thickness caused by single stomata [15] and on hydrodynamically based models on the estimation of the boundary layer thickness of perfectly flat plant leaves [4, 16]. This

altogether leads to a demand for applied analytical techniques to investigate the boundary layer structures and their dynamics.

Available extractive gas sampling techniques destroy the spatial structure of the CBL and are therefore not suited to resolve the small scales of the spatial heterogeneity. Further, as stomata opening reacts on changes of the air humidity [17], gas sampling inevitably leads to systematic errors and may cause non-quantifiable feedback on the transpiration patterns of the biological system. In addition, extractive techniques do not provide the required temporal resolution defined by the reaction time of the plant leaf [18]. As the estimated boundary layer thickness of <15 mm under static conditions is too small for the available measurement techniques [19], a wind speed-dependent investigation of the H_2O CBL structure was out of reach for state-of-the-art extractive measurement techniques. These constraints necessitate a non-intrusive H_2O vapour measurement technique with high temporal and spatial resolution.

A laser-based, optical in situ gas analysis technique called **Tunable Diode Laser Absorption Spectroscopy** (TDLAS) is a promising alternative which could provide sufficient spatial and temporal resolution needed for a dynamic, spatially resolved investigation of the thin water vapour boundary layer of a plant leaf.

Recently, we developed set-ups to enable 1D spatially resolved studies of the transpiration of single plant leaves using fibre-coupled multichannel TDLAS at 1.4 μm [20]. These set-ups were based on static, simultaneously measuring, multichannel laser-detector arrangements. These were designed for the investigation of the dynamics of spatial transpiration structures and their dependence on variations in light-shadow conditions [21] in a plane parallel to the leaf surface. The vertical structure of the water vapour boundary layer was not studied so far with sufficient spatial resolution.

With the development of GaInAsSb-/GaSb-based DFB diode lasers emitting in the wavelength region up to 2.84 μm [22], strong ro-vibrational H_2O transitions in the fundamental ν_1 and ν_3 vibration bands became accessible for high-sensitivity TDLAS-based gas analysis. These 2.7- μm band lines are up to 20-fold stronger than the strongest transitions in the commonly used $2\nu_1$, $2\nu_3$, $\nu_1 + \nu_3$ combination and overtone bands. This feature has already been used to develop very compact spectrometers for H_2O vapour detection and temperature measurements in combustion processes [23], atmospheric H_2O concentration measurements for planetary missions [24–26] and promise high signal-to-noise ratios for enhanced concentration resolution on very short absorption paths, necessary for spatially resolved measurements.

In contrast to previous work on 2.7 μm TDLAS, where solely static spectrometers without spatial resolution were

constructed, we present in this work the first spatially resolving 2.7 μm TDLAS spectrometer based on a single DFB diode laser and only one stationary InAs detector. Further, we describe our new laminar wind tunnel for single leaves. Combining both, we investigated the dynamics of the H₂O boundary layer structure of single plant leaves and its dependence on the wind speed to provide more insight to these important gas exchange processes.

The importance of understanding the dynamic interaction of stomata with the environment has been expressed by numerous authors, and stomata play a key role in controlling terrestrial environment, e.g. see review by Berry et al. [27]. There is a dynamic coupling of leaf physiology with aerodynamics, probably a good example demonstrating this relation is the Ball-Berry equation [28] which links stomatal conductance and assimilation rate to the humidity on the leaf surface, i.e. directly within the boundary layer. While there are several models used to predict stomatal conductance, usually the Ball-Berry approach has been included as a submodel to estimate the interaction of plants with the environment from a leaf to ecosystem and global scale, e.g. it is used in daily weather prediction and to simulate future climate [29]. The Ball-Berry model is used because of its simplicity and rather reliable predictive value. However, it lacks mechanistic understanding. Stomata may be strongly affected by their closest environment which is determined by the leaf interior and the boundary layer [12]. To test this hypothesis, measurements within the boundary layer are required. Furthermore, despite the physiological control of gas exchange of leaves favoured by biologist, meteorologists usually neglect stomatal control mechanisms in particular with respect to rates of transpiration. The assumption is that when under a certain rate of transpiration, the stomata open transpiration transiently increases transporting humidity into the boundary layer which in turn reduces the vapour gradient between the leaf and boundary layer so that transpiration comes back to the initial value [30].

Solving the problem of the level control of gas exchange of leaves by stomata is a seminal future work needed to improve the prediction of the interaction of vegetation with the environment [31]. Quantitative measurement of exchange processes within the boundary layer will thus provide the necessary tools, and the presented work is an important step to enable measurement of water vapour within the boundary layer. In particular, the close cooperation between physicists, biologists and meteorologists will provide the possibility to test existing models and improve them with experimental in situ measurements within the boundary layer.

2 Experimental set-up

Our measurements on the dynamics of the H₂O boundary layer structures on single plant leaves require a rapidly sequentially scanning in situ TDLAS spectrometer with optimized spectroscopic and mechano-optic characteristics (i.e. an optimized absorption line selection), as well as a matching electronics set-up, i.e. a high-speed data acquisition procedure and a dedicated optical scanning set-up, with controlled beam quality, alignment and displacement. Furthermore, the atmospheric boundary conditions around the leaf have to be controlled precisely, i.e. controlled air and leaf temperature, air humidity and gas flow close to the leaf surface. Finally, all building blocks had to be combined into one set-up.

2.1 TDLAS detection of water vapour at 2.7 μm

The gas analysis technique of TDLAS is based on the absorption of narrowband, single-mode laser light by gaseous absorbers and described by the extended Lambert-Beer law

$$I(v(t)) = I_0 \cdot Tr(t) \cdot \exp(-S(T) \cdot \phi(v(t) - v_0) \cdot nL) \quad (1)$$

Here, $I_0(v(t))$ denotes the intensity of incident laser light and $I(v(t))$ the light intensity after the passage through the measurement volume of length L , containing absorber molecules at an absorber density n . For a given transition, $S(T)$ is the line strength of the ro-vibrational transition at the gas temperature T . The line-shape function $\phi(v(t) - v_0)$ is normalized to a surface area of 1 and depends on the collision model [32–34] to describe the spectral line profile around the absorption line centre at v_0 [cm⁻¹]. $Tr(t)$ accounts for potential broadband transmission changes in the measurement volume, whereas $E(t)$ is the time-varying background radiation reaching the detector. By resolving the Lambert-Beer law [Eq. (1)] with respect to n and spectrally integrating over the absorption line profile, the absorber concentration density can be calculated by

$$n = -\frac{1}{S(T) \cdot L} \int \left(\frac{I(v(t)) - E(t)}{I_0(v(t)) \cdot Tr(t)} \right) \frac{\partial v(t)}{\partial t} dt \quad (2)$$

Eq. (2) indicates that the number density n can be calculated without any need of signal calibration. Thus, for an absolute concentration measurement, we only need a precise knowledge of the line strength $S(T)$, the experimental boundary conditions L [m], T [K] and p [mbar] as well as $Tr(t)$ and $E(t)$, which can be determined from the raw signal. The absorption line area is derived from a spectral scan over the absorption line by modulating the laser current using a triangular-shaped current ramp provided by a function generator with a fixed modulation frequency

Fig. 1 Line strengths of H₂O molecule in the NIR range from 1 – 3 μm (296 K), based on the HITRAN04 database. The paper focuses on the ν_1 , ν_3 absorption band at 2.7 μm

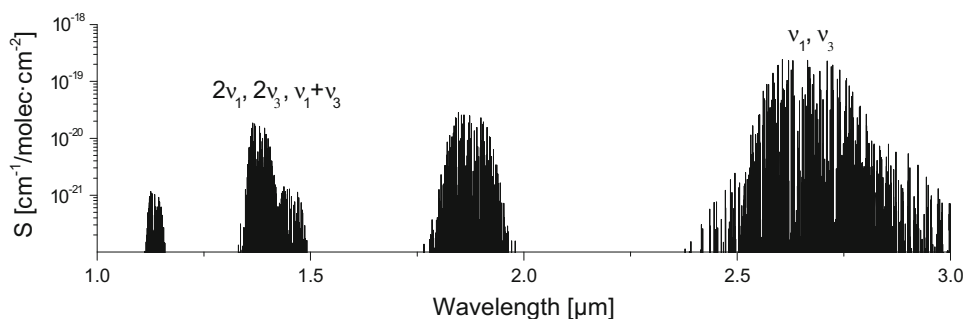


Table 1 HITRAN04 data of the absorption lines used to calculate the H₂O concentration in the leaf's boundary layer

Central wavelength ν_0 [cm ⁻¹]	Line strength S(293 K) [cm ⁻¹ /(molec·cm ⁻²)]	Air pressure broadening [1/(cm·atm)]	Pressure broadening [1/(cm·atm)]	Ground state energy E'' [cm ⁻¹]
3,619.611	$8.351 \cdot 10^{-20}$	0.0862	0.4291	446.5107
3,619.91609	$2.142 \cdot 10^{-21}$	0.1126	0.1200	37.1371
3,620.04076	$6.011 \cdot 10^{-23}$	0.0820	0.4815	414.1681

around the average laser current. The additional parameter in Eq. (2) describes the laser tuning coefficient, i.e. dynamic change of laser wavelength upon rapid variations of the laser operating current.

Diode laser-based water vapour measurements have been demonstrated frequently in the NIR wavelength region around 1.4 μm, where fibre-coupled, telecommunication DFB diode lasers and low-noise detectors are available for reasonable costs. With the advent of room-temperature, DFB diode lasers working at wavelengths up to 2.9 μm [22] the much stronger absorption lines in the ν_1 , ν_3 fundamental vibrational band became accessible (Fig. 1). These stronger absorption features promise increased signal-to-noise ratio, i.e. concentration resolution, under the assumption that the optical noise characteristics remain comparable to 1.4 μm spectrometers.

Typical double extended InGaAs photodetectors show a steep sensitivity cut-off around 2.55 μm, so that the choice of the absorption line and the detector characteristics may strongly influence the spectrometer performance and thus have to be carefully balanced. For this important but tedious task, we developed a semi-automatic line selection software [35] which performs spectral simulations using HITRAN line data [36] to select an optimal absorption line by taking into account the experimental boundary conditions. Particularly, important for this application was a minimized temperature coefficient $S(T)/T$ of the absorption line of 0.1 %/K [19]. Based on the given experimental conditions, i.e. sufficient absorption at short absorption paths, low-temperature coefficient at standard pressure and temperature in the measurement volume, the 523 → 422 (001 → 000) transition at a central wavelength of 3,619.611 cm⁻¹ was found to be the most suitable

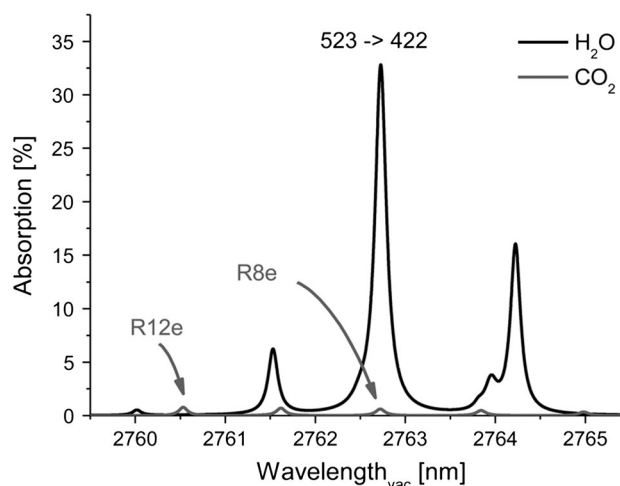


Fig. 2 Simulated absorption spectrum using the HITRAN04 database with ambient concentrations of 10000 ppm H₂O and 380 ppm CO₂ (296 K, 1 atm, 5.4 cm path length)

absorption line for H₂O boundary layer measurements [37] and a corresponding DFB laser (Nanoplus GmbH, Germany) was selected.

For the concentration measurements, the main absorption line, as well as two adjacent H₂O absorption lines, was taken into account for the data evaluation (Table 1).

Assuming an ambient H₂O vapour concentration of 10.000 ppm in direct vicinity of the plant leaf, the selected transition shows an absorption of 33 % (4.03×10^{-1} OD) at an absorption path length of only 5.4 cm (Fig. 2).

The selected 2.76 μm DFB laser emits under standard conditions an optical power of 5.2 mW and exhibits side mode suppression ratio of -28 dB [38], which was measured using an FTIR spectrometer and which is sufficient

for TDLAS concentration measurements under atmospheric conditions.

Another important parameter to be determined is the dynamic tuning coefficient (described in Eq. 2), which can be highly nonlinear and which depends on the laser working point, i.e. the laser temperature, average current and modulation frequency [38–40]. Absolute TDLAS measurements require a precise characterization of the spectral properties of the 2.7 μm laser, including the dynamic tuning coefficient [19] and its dependence on the modulation frequency.

Nonlinear internal relaxation effects cause different functional dependencies of the dynamic tuning coefficient as a function of relative driving current (Fig. 3), thus leading to different modulation depths. We measured the modulation frequency-dependent tuning coefficients using a Ge etalon ($L = 2.54$ cm) and a semi-automated fringe fitting software. At a modulation frequency of 500 Hz and current amplitude of 56 mA, the laser is able to scan a spectral range of ≈ 1.2 cm^{-1} which is sufficient for probing the selected ro-vibrational H₂O absorption line under ambient pressure and temperature conditions.

2.2 Optical and electrical set-up

The electronic part of the spectrometer set-up consists of a function generator providing a continuous, periodic, triangular voltage signal at a modulation frequency of 500 Hz to the laser driver, resulting in a ± 56 mA laser current ramp around the average laser current of 100 mA. The open laser chip, which is placed on a TO₅ mount with a built-in Peltier element-based temperature control, was stabilized at a laser operating temperature of 28.5 $^{\circ}\text{C}$.

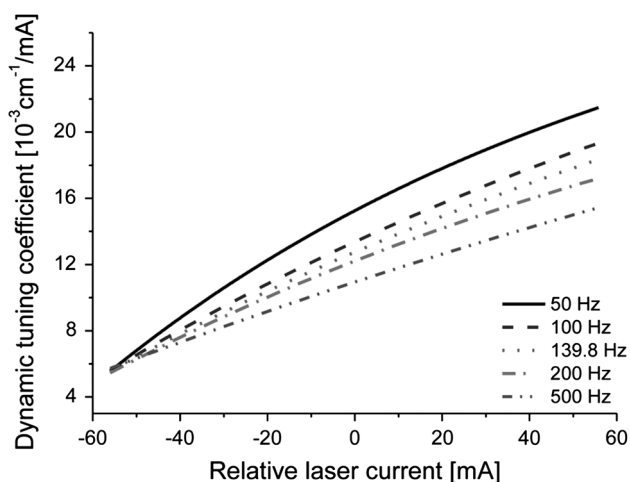


Fig. 3 Measured frequency-dependent, dynamic tuning coefficients as a function of the injection current, around an average current of 110 mA for modulation frequencies from 50 up to 500 Hz

The optical set-up (Fig. 4) starts with an AR-coated plano-aspheric lens [$f = 3.05$ mm, $d = 6.5$ mm, material BD-2 ($\text{Ge}_{28}\text{Sb}_{12}\text{Se}_{60}$)] which was used to focus the laser beam to the centre of a planar galvanometric scanner mirror. The successive off-axis parabolic (OAP) mirror, OAP1 ($f = 76$ mm, 90° , $d = 3''$), (Fig. 4), picks up this divergent beam, collimates it to a 1-mm-diameter ($1/e$ full width) beam and directs it through the leaf chamber which allows an absorption length of 54 mm directly beneath the leaf. The absorption path inside the wind tunnel is separated from the outside air masses via two 100- μm -thin polyethylene foils serving as side “windows” of the leaf chamber. Behind the leaf chamber, the light is picked up by an identical OAP 2, which then focussed the collected laser radiation onto a room-temperature InAs photodetector with 1 mm active diameter.

This combination of a galvanometric scanner and two OAP mirrors allowed to convert the angular excursion of the galvanometric scanner into a parallel transverse displacement of the laser beam, which was used to sense the vertical 1D water vapour profile beneath the leaf. This parallel traversing mechanism takes advantage of the optical properties of the OAP mirror pair and ensures a parallel laser scanning hygrometer suitable for the project task. The vertical step size of the laser beam was set to 0.18 mm and a vertical scan range of 14 mm beneath the leaf was achieved. A full vertical scan of the leaf vicinity took 15.5 s.

The resulting photodetector current was amplified and converted into a voltage signal by a low-noise transimpedance amplifier and digitized with a 500kSamples/s 18-bit A/D-converter. Because the data collection clock and the laser scan clock were not synchronized, the average of direct-absorption data from multiple scans required the adjustment (± 1 pixel) to align the absorption features. The H₂O concentrations were calculated for each mirror position using our LabView-based fitting routine [41].

To minimize the effect of unwanted parasitic H₂O absorption along the laser path outside the measurement zone under the leaf, the whole optical set-up was placed in a sealed environment and constantly purged with dry air with a dew point of -70 $^{\circ}\text{C}$ (2.6 ppm, 0.009 % relative humidity). Nevertheless, due to water adsorption on the wall of the sealed volume or leaks in the containment, the minimum H₂O concentration within the purged volume was determined to be approximately 293 ± 5 ppm, which corresponds to a dew point of -32 $^{\circ}\text{C}$ and a relative humidity of 1.1 % at 23 $^{\circ}\text{C}$. This “background” H₂O concentration was achieved after a 2-h purging time and was found to be constant throughout the whole duration time of the measurements. For the analysis of the vertical concentration gradients, this absorption signal was taken to be constant and subtracted from all resulting H₂O concentration data.

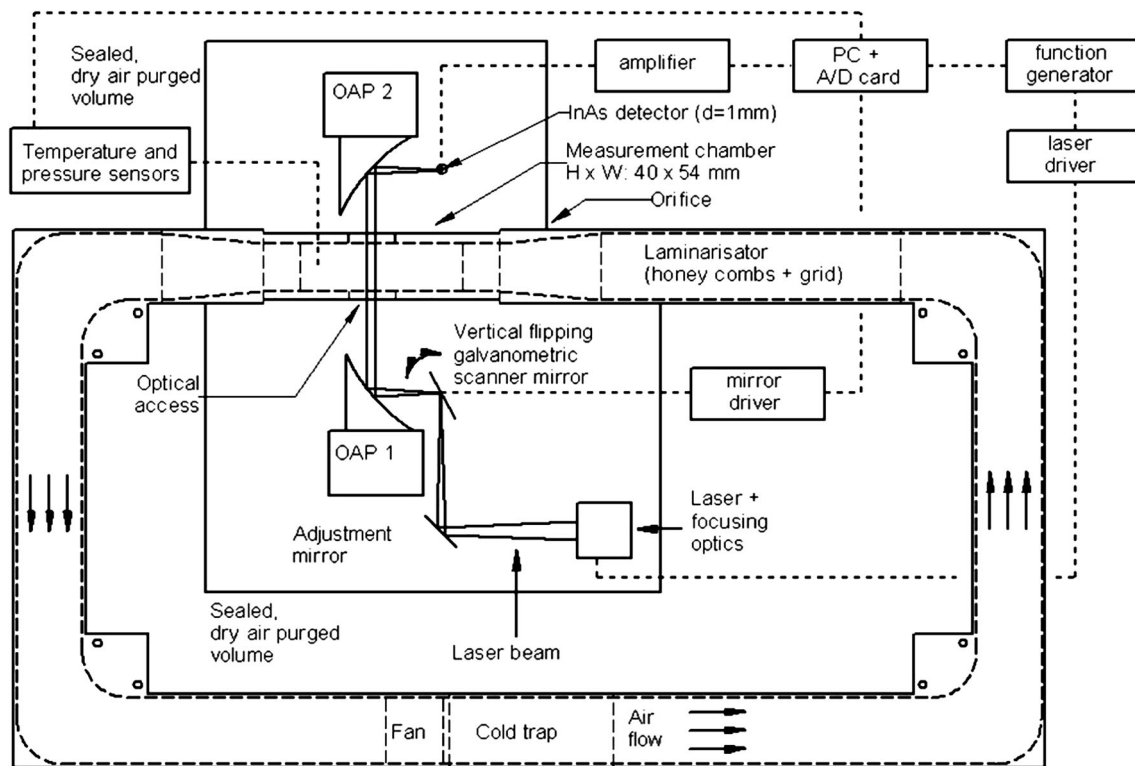


Fig. 4 Top view of the complete experimental set-up for H_2O boundary layer measurements consisting of closed wind tunnel, purged laser optics, electronics and data acquisition system

2.3 Wind tunnel set-up

As the leaf transpiration rate, stomatal opening and the corresponding H_2O fluxes are greatly influenced by H_2O concentration of the ambient air surrounding the leaf, the gas composition inside the measurement chamber has to be kept constant. This is even more important as naturally occurring temporal fluctuations in ambient water vapour concentrations can mask or falsify the measured H_2O vertical structure. In addition, the flow field under the leaf surface has to be spatially homogeneous and laminar with an adjustable wind speed. This task was solved via the construction of a novel wind tunnel for leaf transpiration studies, i.e. a closed-loop aluminium wind tunnel, sealed from ambient air (Fig. 4). The whole wind tunnel is table top mounted with an overall dimension of 0.72 m^2 ($1.2 \text{ m} \times 0.6 \text{ m}$) and a weight of 25 kg.

To maintain constant wind speeds, an axial fan was placed inside the wind tunnel, capable of generating constant but adjustable wind speeds from 0.1 to 6 m/s. The propelled air was guided through a specially designed, peltier-cooled cold trap to extract excess water vapour emitted by the leaf and to keep the background H_2O concentration within the wind tunnel at a constant level. Laminarization of the flow and homogenization of flow speed were achieved by a sequential arrangement of

aluminium honeycombs ($l = 6 \text{ cm}$, $d = 3.2 \text{ mm}$) and a specially designed flow compressing orifice directly upstream the leaf measurement chamber. The honeycombs created a laminar flow for air speeds up to 4 m/s and filtered out large-scale turbulence. We removed the typical parabolic wind speed profile close to the wind tunnel walls by continuous reduction in the rectangular tunnel cross section from an innertube cross-sectional area of $72 \times 72 \text{ mm}$ ($5,184 \text{ mm}^2$) to $54 \times 40 \text{ mm}$ ($2,160 \text{ mm}^2$) and an associated compression of the air flow. In addition, this set-up assures minimized small-scale turbulence by dissipation of the small-scale turbulence downstream of the honeycomb section [42].

The 2D flow field in the measurement section was characterized for different wind speeds with a spatial resolution of 1 mm in vertical and horizontal direction using a heat wire anemometer (probe diameter 1 mm, measurement frequency 4 Hz) mounted on a traversing stage and was found to be quite homogeneous (Fig. 6, left).

The temporal fluctuations at several locations inside the chamber were found to be less than the anemometer's instrumental resolution of 3 cm/s. An analysis of the relative frequencies distribution of the flow speeds, exemplarily, is shown in Fig. 5 for a selected wind speed, with an adjusted binning interval of 0.031 m/s [43] revealed an average velocity of 0.42 m/s and a total flow

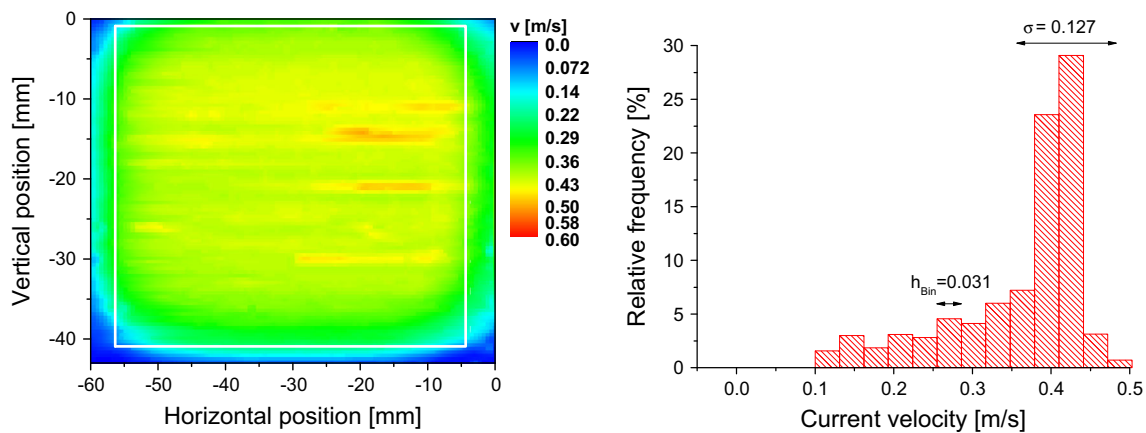


Fig. 5 Exemplary 2D velocity field inside the measurement chamber. Inside the measurement volume (white frame), an average wind speed of 0.42 m/s with a total current distribution width of only 0.13 m/s is generated

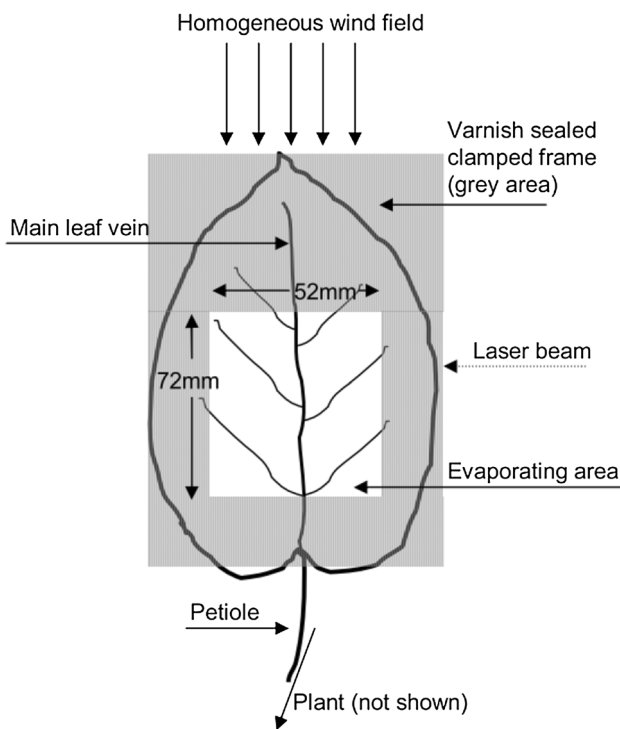


Fig. 6 Bottom side (stomatous side) view of the leaf fixing on top of the measurement chamber. This set-up prevented leaf fluttering and provided a flat leaf surface. The grey area shows the bottom side of the metallic clamp with a thickness of 0.1 mm. The leaf area in the clamp was sealed with water-free varnish to prevent parasitic water vapour evaporation

speed fluctuation of 0.13 m/s (1σ). Despite the apparent high current fluctuation in the chamber, the frequency distribution of the velocities showed a sharp peak with a full width of only 0.13 m/s, containing 51 % of the current velocities, whereas the fraction of the lower velocities originated from friction effects caused by the inner walls of the wind tunnel (Fig. 5, right). Further, we validated the

quality of the flow field by calculating the homogeneity [44] and found a constant relative homogeneity for all investigated flow fields around 0.969 ± 0.03 (maximum homogeneity equals 1). This high homogeneity in addition with the prominent peaks in the velocity histogram is a strong evidence for negligible spatial velocity gradients and thus for a good laminarity on the resolved scale of 1 mm.

The air temperature in the measurement chamber was measured by a calibrated Type-E Class 1 thermocouple within an absolute accuracy of 0.1 K, which was mounted 5 mm beneath the leaf surface on the lee side of the laser beam position to avoid turbulence formation in the light path. During our experiments, the ambient temperature was set to a constant level of 22.9 ± 0.4 °C. Pressure was monitored by a pressure transducer with an absolute accuracy of ± 0.3 hPa at the bottom of the measurement chamber.

The optical measurement area with an internal rectangular cross section of 44×52 mm ($h \times L_{\text{abs}}$) could be accessed through a window and allowed a maximum vertical scanning range of 26 mm beneath the plant leaf. The leaf, which was always kept alive and attached to the plant, was carefully clamped in a thin metal frame, resulting in an evaporative area of 3744 mm² (72 mm \times 52 mm) (Fig. 6).

By mounting the frame on top of the open measurement volume with a horizontal surface orientation and the stomatous side pointing downward, the wind tunnel was sealed from ambient air and only H₂O vapour from the leaf could be emitted into the measurement volume. This frame also prevented the leaf from fluttering in the airstream to achieve a laminar flow structure close to the surface as possible and to keep the leaf surface area at a fixed position. This construction enabled distortion-free H₂O concentration measurements for the first time as close as 0.7 mm to the leaf surface.

To trigger photosynthetic activity, the upper side of the leaf (plant: *Epipremnum pinnatum* var. Golden Pothos) was illuminated with an LED light source which was placed 12 cm above the leaf. This special, circular LED-array emitted photosynthetic actinic light with two intensity maxima in the photosynthetic active wavelength regions of the chlorophyll molecule around 425–500 and 630–700 nm to activate photosynthesis processes, which initiate stomata opening and transpiration. While the reduced thermal radiation of an LED-based illumination minimized thermal influences, the distance of 12 cm was a compromise between photon flux density and homogeneous light conditions on the leaf's surface. This set-up minimized the thermal effects which could otherwise influence gas temperature in the measurement volume (causing spectral problems) as well as the leaf temperature (influencing the transpiration).

In previous works [20], it was found that even dark neighbouring parts of the illuminated leaf areas show transpiration. To prevent the concentration measurements from uncontrollable and parasitic evaporation, the unilluminated leaf parts were sealed with water-free varnish.

2.4 Evaluation of the 2.7 μm TDLAS spectrometer

In order to process the TDLAS raw scans, they had to be transformed from the time regime into the wavenumber regime, which is done by inverting the dynamic wavelength tuning data. Removal of the base line of the raw signal was achieved by dividing the detector signal by a polynomial baseline using a nonlinear Levenberg–Marquardt-fitting algorithm to yield the absorption line profile on an OD scale. Here, we used a second-order baseline polynomial in combination with a Voigt absorption line-shape model with calculated Doppler width, derived from the measured gas temperature and molecular mass. This procedure then revealed the line-of-sight averaged H_2O vapour concentration (Fig. 7). By fitting the absorption line profile using HITRAN04 parameters for line strength, self and foreign broadening and applying the ideal gas law with measured values for pressure, temperature and absorption path length, we extracted the absolute H_2O concentration according to Eq. (2).

By applying a multi-line Voigt fit including the $422 \rightarrow 523$ transition and the two adjacent H_2O transitions $000 \rightarrow 111$, $331 \rightarrow 422$, a line-of-sight average of the H_2O concentration was derived. This average included the sealed and N_2 -purged optics containment where 1,140 ppm was measured. Correcting for this parasitic absorption, we determined a H_2O concentration of 14,670 ppm in the measurement chamber. The residual structure of the fit, i.e. the difference between measured line profile data and the line-shape model, was used to estimate the spectrometer

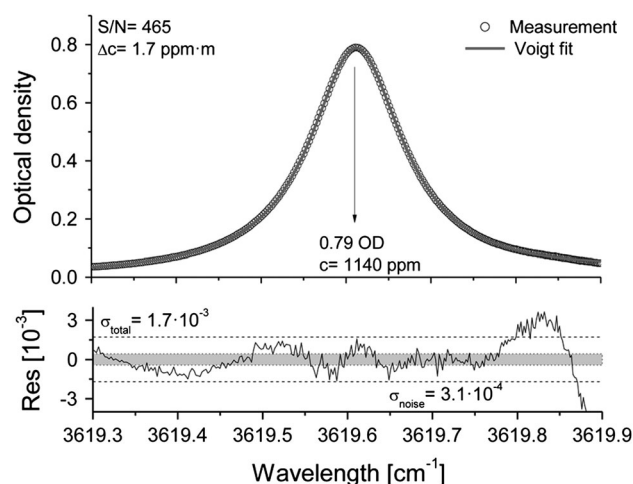


Fig. 7 Typical processed absorption signal and residual structure during a measurement at a wind speed of $0.1 \text{ m}\cdot\text{s}^{-1}$. Concentrations are obtained by fitting the main absorption line structure ($422 \rightarrow 523$) and two neighbouring absorption lines ($000 \rightarrow 111$, $331 \rightarrow 422$) around a central wave number of $3,619.61 \text{ cm}^{-1}$

resolution. During the vertical shift of the laser beam, the standard deviation (1σ) of the global residual structure was found to be at a constant level of 1.7×10^{-3} . At a peak absorption of 0.79 OD, the signal-to-noise of 465 gave a normalized concentration resolution of $1.7 \text{ ppm}\cdot\text{m}$, respectively, 31 ppm for 5.4 cm absorption length. As the low-frequency part of the residual structure remained stable at all spatial positions, we could apply our background reduction procedure [38] and identify the noise dominated residual level to be 3.1×10^{-4} , giving a signal-to-noise ratio of 2,500. Using this SNR, we compute a H_2O precision of 6 ppm based on the absorption path length inside the leaf chamber, which converts into a normalized concentration resolution of 314 ppb·m.

2.5 Evaluation of the leaf chamber

In order to validate the experimental set-up with regard to the measured vertical H_2O concentration gradients and concentration profiles, we analysed the spectrometer characteristics with a dark-adapted plant leaf at zero wind speed. Therefore, we mounted the leaf on top of the measurement chamber in darkness and under ambient environmental conditions. To avoid photosynthetic activity of the leaf and to ensure that stomatal opening was minimal, the whole set-up, including the complete plant, was placed in darkness 3 h before start of the measurement procedure. The optical set-up outside the leaf chamber was purged with dry air 3 h before concentration measurements in order to obtain a stable background concentration level outside the measurement volume. Complete mixing of the air volume within the wind tunnel with a completely dark-

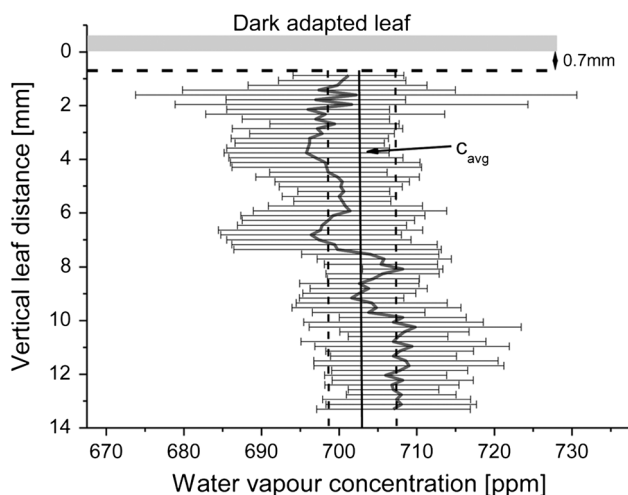


Fig. 8 Vertical H₂O concentration profile with a dark-adapted leaf under static conditions inside the measurement chamber

adapted leaf was achieved with a low air flow ($v_{\text{air}} = 0.2 \text{ m/s} \leftrightarrow V_{\text{air}}/t = 432 \text{ cm}^3/\text{s}^1$). To ensure static conditions, the air flow was stopped 2 min before the vertical concentration profile measurements were started.

Four consecutively sampled vertical H₂O concentration profiles under a fully dark-adapted leaf were averaged during completely static air conditions in the tunnel. Subtraction of the stable background concentration yielded within the error bars a homogenous, vertical H₂O profile with an average concentration of $702 \pm 4 \text{ ppm}$. This accounts for a vertically mixed H₂O concentration field inside the measurement chamber of $9,070 \pm 50 \text{ ppm}$. The relative standard deviation at each measurement point of the vertical profile is only 1.4 % during four vertical scans (Fig. 8). Subsequently, performed measurements at a maximum air velocity of 0.9 m s^{-1} and identical environmental conditions revealed slight temporal changes in the measured concentration profiles with a line-of-sight integrated fluctuation of $\pm 11 \text{ ppm}$, which resulted in concentration fluctuations of only 140 ppm inside the measurement chamber during the overall sampling time of 64 s.

3 Measurements and results

As stomatal opening and water vapour emission rates follow photosynthetic activity with a time lag of approximately 20 min in *E. pinnatum* [45], a constant CBL structure cannot be measured before reaching a steady state of evaporation. These variations before the steady state clearly show the dynamic functional adjusting of stomatal opening to the experimental light conditions. After reaching steady-state conditions (1 h after start of illumination),

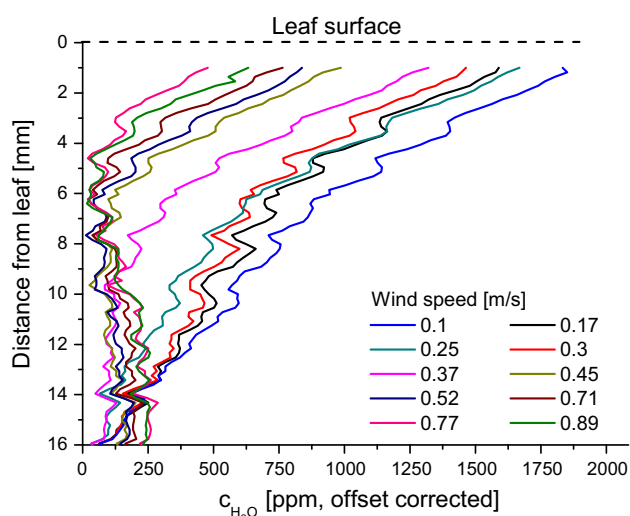


Fig. 9 Wind speed dependence of the vertical H₂O vapour boundary layer structure of the photosynthetic active plant leaf

we could scan the vertical concentration profiles of water vapour beneath the leaves (Fig. 10).

For each selected wind speed, the H₂O vapour concentration profiles were determined by averaging four consecutive vertical profiles. To cope with the problem of the slowly increasing water vapour background, caused by the continuous transpiration of the leaf into the closed-loop wind tunnel, each averaged vertical profile was normalized to the point of lowermost concentration, i.e. the smallest concentration value was subtracted from the corresponding profile.

This yields to a better direct comparison of the wind speed influence to the spatial structure of the CBL. Choosing ten different wind speeds in the range from 0.1 to 0.9 m/s, the influence of the wind speed to the profile structure could be clearly detected (Fig. 9). Between changes of the wind speed, a time of 2 min was set to reach a new steady state conditions. Compared to our previous profile measurements at zero wind speed [38], the now achieved temporal resolution increased by a factor of 20 at a comparable spatial resolution and at much better controlled boundary conditions.

With increasing wind speeds, the H₂O vapour concentration at the surface decreases. We assign this concentration change to a reaction of the leaf evaporation on the changed wind speed. All vertical profiles show two separated nearly linear parts with different concentration gradients. While for slow wind speeds up to 0.3 m/s, the transition between the leaf's nearby gradients and far-out gradients tend to be smooth, the differences are far more evident for wind speeds exceeding 0.3 m/s. For those wind speeds, still nonzero concentration gradients in the nearby region are present; the water vapour concentrations in the

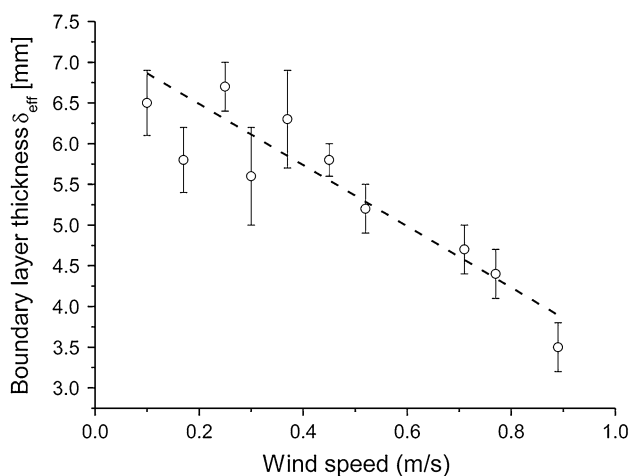


Fig. 10 Wind speed-dependent H₂O vapour boundary layer thickness compared with a linear decreasing fit model

far-out are constant within the measurement accuracy. Due to the horizontal laminar flow in the measurement chamber, vertical H₂O vapour transport is governed by diffusion processes. According to [46], the thickness of the CBL can be determined by Nernst's method.

As the dimensions of the nonzero gradient parts close to leaf surface decline with increasing wind speed, the boundary layer thickness also decreases (Fig. 10). We could extract boundary layer thicknesses for wind speeds up to 0.9 m/s. The boundary layer thickness in our wind tunnel measurements is 6.5 ± 0.5 mm for very low wind speeds of 0.1 m/s and thus in good accordance with the result measured previously under static conditions (6.7 ± 0.5 mm) [38]. This boundary layer thickness drops linearly down to 3.5 mm with increasing wind speed. For higher wind speeds, the boundary layer structure was not resolvable within the spectrometer's resolution and only a mixed gas column was detected (Fig. 9).

4 Conclusion

Applying the principles of wind tunnel design on a small scale in combination and combining it with a new, spatially scanning, open-path TDLAS hygrometer at 2.7 μm , we achieved to investigate the spatially resolved boundary layer dynamics of a single transpiring plant leaf. The new system is based on a 2.7- μm DFB diode laser. To cope with the dynamic properties of the leaf's boundary layer structure, we developed a laser-detector set-up that uses galvanometric scanner mirrors to allow (within a time of 16 s) a vertical laser beam displacement (scanning range) of 13 mm at a spatial resolution (step size of the vertical laser beam displacement) of 0.18 mm. This set-up thus permits a

spatially resolved high-speed concentration measurement with only one stationary mounted detector. The TDLAS hygrometer with an absorption path length of only 5.4 cm showed a concentration resolution of 315 ppbV·m, which we used to measure H₂O concentration gradients down to 120 ppmV/mm, as well as the dependence of the boundary layer shape on different wind speeds in the range 0.1–0.9 m/s. The smallest boundary layer thickness measured was 3.5 mm at our highest wind speeds.

The developed scanning approach can be easily modified for applications where water vapour concentration gradients have to be resolved perpendicular to laser beam axis. Moreover, it may (using a second galvo scanner) also be extended to the measurement of two-dimensional water vapour concentration fields or may be combined with spatially resolved thermography and/or chlorophyll fluorescence methods for a more detailed understanding of water vapour evaporation from leaves and the linked photosynthetic processes.

References

1. M. Alistair, F. Hetherington, F.I. Woodward, The role of stomata in sensing and driving environmental change. *Nature* **424**, 901–908 (2003)
2. W. Cramer, A. Bondeau, F.I. Woodward, I.C. Prentice, R.A. Betts, V. Brovkin, P.M. Cox, V. Fisher, J. Foley, A.D. Friend, C. Kucharik, M.R. Lomas, N. Ramankutty, S. Sitch, B. Smith, A. White, C. Young-Molling, Global response of terrestrial ecosystem structure and function to CO₂ and climate change: results from six dynamic global vegetation models. *Glob. Change Biol.* **7**, 357–373 (2001)
3. D. Gerten, S. Schaphoff, W. Lucht, *Clim. Change* **80**, 277–299 (2007)
4. P.S. Nobel, *Physiochemical and environmental plant physiology* (Academic Press, USA, 2005)
5. D.D. Baldocchi, Assessing the eddy covariance technique for evaluating carbon dioxide exchange rates of ecosystems: past, present and future. *Glob. Change Biol.* **9**, 479–492 (2003)
6. U. Schreiber, H. Hormann, C. Neubauer, C. Klughammer, Assessment of photosystem ii photochemical quantum yield by chlorophyll fluorescence quenching analysis. *Aust. J. Plant Physiol.* **22**, 209–220 (1995)
7. U. Rascher, R. Pieruschka, Spatio-temporal variations of photosynthesis: the potential of optical remote sensing to better understand and scale light use efficiency and stresses of plant ecosystems. *Precis. Agric.* **9**, 355–366 (2008)
8. R. Pieruschka, D. Klimov, Z. Kolber, J.A. Berry, Continuous measurements of the effects of cold stress on photochemical efficiency using laser induced fluorescence transient (LIFT) approach. *Funct. Plant Biol.* **37**, 395–402 (2010)
9. A. Damm, J. Elbers, A. Erler, B. Gioli, K. Hamdi, R. Hutjes, M. Kosvancova, M. Meroni, F. Miglietta, A. Moersch, J. Moreno, A. Schickling, R. Sonnenschein, T. Udelhoven, S. van der Linden, P. Hostert, U. Rascher, Remote sensing of sun-induced fluorescence to improve modeling of diurnal courses of gross primary production (GPP). *Glob. Change Biol.* **16**, 171–186 (2010)

10. E.-D. Schulze, M.M. Caldwell, *Ecophysiology of photosynthesis. Ecological Studies, 100* (Springer Berlin, Heidelberg, 1995)
11. J.C. Shope, D. Peak, K.A. Mott, Stomatal responses to humidity in isolated epidermes. *Plant Cell Environ.* **31**, 1290–1298 (2008)
12. R. Pieruschka, G. Huber, and J. A. Berry, “Control of transpiration by radiation,” in: *Proceedings of the National Academy of Sciences* **107**, (2010)
13. U. Schurr, A. Walter, U. Rascher, Functional dynamics of plant growth and photosynthesis—from steady-state to dynamics—from homogeneity to heterogeneity. *Plant Cell Environ.* **29**, 340–352 (2006)
14. J. Grace, J. Wilson, The boundary layer over a *Populus* Leaf. *J. Exp. Bot.* **27**, 231–241 (1975)
15. J.R. Troyer, Diffusion from a circular stoma through a boundary layer—a field theoretical analysis. *Plant Physiol.* **66**, 250–253 (1980)
16. P.H. Schuepp, Tansley review no. 59 Leaf boundary layers. *New Phytol.* **125**, 477–507 (2006)
17. O.L. Lange, R. Rösch, E.D. Schulze, L. Kappen, Responses of stomata to changes in humidity. *Planta* **100**, 76–86 (1971)
18. L. Fanjul, H.G. Jones, Rapid stomatal responses to humidity. *Planta* **154**, 135–138 (1982)
19. K. Wunderle, S. Wagner, and V. Ebert, “2.7 μm DFB Diode Laser Spectrometer for Sensitive Spatially Resolved H₂O Vapor Detection,” in *LACSEA*, (2008)
20. S. Hunsmann, *Fasergekoppelte Mehrkanal-Laser-Hygrometer zur in situ Messung der globalen und lokalen Transpirationsdynamik einzelner Pflanzenblätter* (Universität Heidelberg, Physikalisch-Chemisches Institut, 2009)
21. S. Hunsmann, K. Wunderle, S. Wagner, U. Rascher, U. Schurr, V. Ebert, High resolution measurements of absolute water transpiration rates from plant leaves via 1.37 μm tunable diode laser absorption spectroscopy (TDLAS). *Appl. Phys. B* **92**, 393–401 (2008)
22. M. Hümmer, K. Rößner, T. Lehnhardt, M. Müller, A. Forchel, R. Werner, M. Fischer, J. Koeth, Long wavelength GaInAsSb-AlGaAsSb distributed-feedback lasers emitting at 2.84 μm . *Electron Lett.* **42**, 583–584 (2006)
23. A. Farooq, J.B. Jeffries, R.K. Hanson, In situ combustion measurements of H₂O and temperature near 2.5 μm using tunable diode laser absorption. *Meas. Sci. Technol.* **19**, 075604 (2008)
24. C.G. Tarsitano, C.R. Webster, Multilaser Herriott cell for planetary tunable laser spectrometers. *Appl. Opt.* **46**, 6923–6935 (2007)
25. G. Durry, J.S. Li, I. Vinogradov, A. Titov, L. Joly, J. Cousin, T. Decarpenterie, N. Amarouche, X. Liu, B. Parvitte, O. Korablev, M. Gerasimov, V. Zeninari, “Near infrared diode laser spectroscopy of C₂H₂, H₂O, CO₂ and their isotopologues and the application to TDLAS, a tunable diode laser spectrometer for the martian PHOBOS-GRUNT space mission,”. *Appl. Phys. B* **99**, 339–351 (2010)
26. G. Durry, L. Joly, T. Le Barbu, B. Parvitte, V. Zéninari, Laser diode spectroscopy of the H₂O isotopologues in the 2.64 micron region for the in situ monitoring of the Martian atmosphere. *Infrared Phys. Technol.* **51**, 229–235 (2008)
27. J.A. Berry, D.J. Beerling, P.J. Franks, Stomata: key players in the earth system, past and present. *Curr. Opin. Plant Biol.* **13**, 232–239 (2010)
28. J.T. Ball, I.E. Woodrow, J.A. Berry, “A model predicting stomatal conductance and its contribution to the control of photosynthesis under different environmental conditions,” in *Progress in Photosynthesis Research*, vol. IV (Martimis Nijhoff Publishers, Dordrecht, 1987), pp. 221–224
29. D. Niyogi, K. Alapaty, S. Raman, F. Chen, Development and evaluation of a coupled photosynthesis-based gas exchange evapotranspiration model (GEM) for mesoscale weather forecasting applications. *J. Appl. Meteorol. Climatol.* **48**, 349–368 (2009)
30. P.G. Jarvis, K.G. McNaughton, Stomatal control of transpiration: scaling up from leaf to region. *Adv. Ecol. Res.* **15**, 1–49 (1986)
31. J.A. Berry, D.J. Beerling, P.J. Franks, Stomata: key players in the earth system, past and present. *Curr. Opin. Plant Biol.* **13**, 232–239 (2010)
32. L. Galatry, Simultaneous effect of Doppler and Foreign Gations of broadening on spectral lines. *Phys. Rev.* **122**, 1218–1223 (1961)
33. S.G. Rautian, I.C. Sobel'man, The effect of collisions on the Doppler broadening of spectral lines. *Sov. Phys. Usp.* **9**, 701–716 (1967)
34. B.H. Armstrong, Spectrum line profiles: the Voigt function. *J. Quant. Spectrosc. Radiat. Transf.* **7**, 61–88 (1967)
35. K. Wunderle, T. Fernholz, V. Ebert, Selektion optimaler Absorptionslinien für abstimmbare Laserabsorptionsspektrometer. *VDI Ber.* **1959**, 137–148 (2006)
36. L.S. Rothman, D. Jacquemart, A. Barbe, D.C. Benner, M. Birk, L.R. Brown, M.R. Carleer, J. Chackerian, K. Chance, L.H. Coudert, V. Dana, V.M. Devi, J.M. Flaud, R.R. Gamache, A. Goldman, J.M. Hartmann, K.W. Jucks, A.G. Maki, J.Y. Mandin, S.T. Massie, J. Orphal, A. Perrin, C.P. Rinsland, M.A.H. Smith, J. Tennyson, R.N. Tolchenov, R.A. Toth, J. Vander Auwera, P. Varanasi, G. Wagner, “The HITRAN 2004 molecular spectroscopic database,”. *J. Quant. Spectrosc. Radiat. Transf.* **96**, 139–204 (2005)
37. K. Wunderle, “Neuartige Konzepte zur schnellen, räumlich aufgelösten Untersuchung der H₂O-Grenzschichtdynamik einzelner Pflanzenblätter und ihrer Abhängigkeit von der Windgeschwindigkeit auf Basis hochempfindlicher 2.7 μm -Laserhygrometer,” Ph.D. Thesis, University of Heidelberg, 2010
38. K. Wunderle, S. Wagner, I. Pasti, R. Pieruschka, U. Rascher, U. Schurr, V. Ebert, Distributed feedback diode laser spectrometer at 2.7 μm for sensitive, spatially resolved H₂O vapor detection. *Appl. Opt.* **48**, B172–B182 (2009)
39. H. Teichert, “Entwicklung und Einsatz von Diodenlaser-Spektrometern zur simultanen in situ-Detektion von CO, O₂ und H₂O in technischen Verbrennungsprozessen,” Dissertation, Ruprecht-Karls Universität, Physikalisch-Chemisches Institut, 2003
40. S. Wagner, B. T. Fisher, J. W. Fleming, and V. Ebert, “TDLAS based *In Situ* Measurement of Absolute Acetylene Concentrations in Laminar 2D Diffusion Flames,” *Proc. Comb. Inst.* **32**, available online <http://dx.doi.org/10.1016/j.proci.2008.05.087> (2008)
41. V. Ebert, H. Teichert, P. Strauch, T. Kolb, H. Seifert, J. Wolfrum, Sensitive in situ detection of CO and O₂ in a rotary kiln-based hazardous waste incinerator using 760 nm and new 2.3 μm diode lasers. *Proc. Comb. Inst.* **30**, 1611–1618 (2005)
42. M.J. Martin, K.J. Scavazze, I.D. Boyd, L.P. Bernal, Design of a low-turbulence, low-pressure wind-tunnel for micro-aerodynamics. *J. Fluids Eng.* **128**, 1045–1052 (2006)
43. D.W. Scott, On optimal and data-based histograms. *Biometrika* **66**, 606–610 (1976)
44. M.-T. Hütt, R. Neff, Quantification of spatiotemporal phenomena by means of cellular automata techniques. *Phys. A* **289**, 498–516 (2001)
45. S. Hunsmann, K. Wunderle, S. Wagner, U. Rascher, U. Schurr, V. Ebert, High resolution measurements of absolute water transpiration rates from plant leaves via 1.37 μm tunable diode laser absorption spectroscopy (TDLAS). *Appl. Phys. B* **92**, 393–401 (2008)
46. R. G. Compton, C. E. Banks, *Understanding Voltammetry*, (World Scientific Pub Co, 2007)